ATR-SEIRAS study of CO adsorption and oxidation on Rh modified Au(111-25 nm) film electrodes in 0.1 M H_2SO_4‡

Qinqin Xu[a2], Antonio Berná[b], Ilya V. Pobelov[a1], Antonio Rodes[b1], Juan M. Feliu[b1], Thomas Wandlowski[a†1], Akiyoshi Kuzume*[a1]

[a]*Department of Chemistry and Biochemistry, University of Bern, Freiestrasse 3, 3012 Bern, Switzerland*

[b]*Departamento de Química Física e Instituto de Electroquímica, Universidad de Alicante, Apartado 99 Alicante, E-03080, Spain*

‡ *This paper is submitted in memory of Professor Thomas Wandlowski, who was a superior scientist, a great mentor and a good friend of us.*

[1]*ISE member*

[2]*Present address: Department of New Energy Science and Engineering, College of Materials & Metallurgy, Guizhou University, Guiyang, 550025, China*

*Corresponding author at: Tel: +41-31-631-4254; Fax: +41-31-631-3993;

E-mail: akiyoshi.kuzume@dcb.unibe.ch (A. Kuzume)

†Deceased

Abstract

Rh modified Au(111-25 nm) electrodes, prepared by electron beam evaporation and galvanostatic deposition, were employed to study adsorption and electro-oxidation of CO

on Rh in 0.1 M sulfuric acid solution by *in situ* attenuated total reflection surface enhanced infrared absorption spectroscopy (ATR-SEIRAS). The results of ATR-SEIRAS experiments were compared with those obtained by infrared reflection absorption spectroscopy on three low-index Rh single crystal surfaces. The Rh film deposited on Au(111-25 nm) electrode consists of 3D clusters forming a highly stepped [n(111) × (111)]-like surface with narrow (111) terraces. When CO was dosed at the hydrogen adsorption potential region, CO adsorbed in both atop (CO_L) and bridge (CO_B) configurations, as well as coadsorbed water species, were detected on the Rh film electrode. A partial interconversion of spectroscopic bands due to the CO displacement from bridge to atop sites was found during the anodic potential scan, revealing that there is a potential-dependent preference of CO adsorption sites on Rh surfaces. Our data indicate that CO oxidation on Rh electrode surface in acidic media involves coadsorbed water and follows the nucleation and growth model of a Langmuir-Hinshelwood type reaction.

Keywords: Rhodium, CO oxidation, ATR-SEIRAS, IRRAS, thin films, single crystal surfaces

1. Introduction

The adsorption and oxidation of CO on transition metals under electrochemical conditions is an important process for both applied and fundamental surface studies [1,2]. CO is the main poison during the catalytic electro-oxidation of organic fuels on platinum group metals [3-5]. On the other hand, the CO adsorption and oxidation processes are very sensitive to the catalyst's structure and therefore it is frequently employed to monitor surface activity.

As a noble metal applied in three-way automobile catalysts, rhodium is well known to be active in the oxidation of CO [6, 7]. The CO adsorption and oxidation on Rh has been investigated extensively in vacuum as well as in gaseous phases and was found to be a structure sensitive Langmuir-Hinshelwood type reaction [8]. Importantly, the CO molecules adsorbed on different surface sites (atop, bridge, multi-fold) can be distinguished by their vibration frequencies. *In situ* infrared reflection absorption spectroscopy (IRRAS) studies of CO chemisorption and electro-oxidation on the low-index Rh single crystal surfaces by Weaver's group demonstrated a strong dependence of the preferable adsorption site on the surface orientation, CO coverage and applied potential [9-14]. A combined IRRAS and *in situ* scanning tunneling microscopic (STM) study revealed two distinctly different potential-dependent CO adlayer structures on smooth Rh(111) in aqueous electrolyte [15]. At low potential, a CO adlayer with (3×√3)-4CO unit cell with CO coverage (θ_{CO}) equal to 0.67 were identified on STM images, which changed to an adlayer with (2×2)-3CO unit cell corresponding to θ_{CO} = 0.75 at high potentials. The corresponding *in situ* IR spectra indicated the presence of CO molecules bound on both atop and 2-fold bridge sites. In case of the Rh(100) electrode,

based on voltammetric and IRRAS experiments, Chang and Weaver proposed that the electro-oxidation of CO on Rh(100) proceeds via nucleation and growth starting at the periphery of preformed CO islands [14]. Gómez *et al*. [16] studied the role of surface heterogeneities (ordered steps and defects) on the oxidation of CO adsorbed at Rh(111) electrodes and found that the more ordered is the Rh(111) surface, the slower the reaction proceeds. Housmanns *et al*. investigated CO electro-oxidation on "ordered" and "disordered" Rh[*n*(111)–(111)] single crystal electrodes [17-21] and proposed that the CO electro-oxidation follows a Langmuir-Hinshelwood type nucleation and growth mechanism controlled by the slow surface mobility of adsorbed CO. Anions were also shown to play an important role in the CO oxidation mechanism on Rh electrodes [19]. In our electrochemical study of the three low-index Rh single crystal surfaces [22] we demonstrated that the reaction pathway of CO oxidation on all three low-index Rh surfaces proceeds according to the Langmuir-Hinshelwood mechanism and is controlled by the formation of OH_{ads} at steps and defect sites, followed by a complex growth process on terrace sites. At the same time, low surface mobility of CO_{ad} leads to a slow and incomplete CO electro-oxidation on Rh(111).

Rh films (or clusters) deposited on various substrates also display high electrochemical activity [23-27]. Vukovic studied the electrochemical behavior of thin Rh film galvanostatically deposited on titanium and demonstrated that their electrochemically active surface area depends on the current density and electro-deposition time [28]. The IRRAS studies by Inukai *et al*. of the CO adsorption on Rh deposited on Pt(111) and Pt(110) electrodes suggested the two dimensional epitaxial growth of the Rh films on Pt(111) and Pt(110) electrodes [29]. Gómez *et al*. studied the

CO adsorption and oxidation on Rh modified Pt(110) and Pt(100) electrodes using *in situ* FT-IR [30, 31]. These authors found that the spectra of the saturated CO adlayers reflected the presence of the foreign admetal. Later they studied the films of Rh on Pt(111) with the aim to investigate their electrochemical and electrocatalytic properties [32] and demonstrated that the behavior of the first layer of Rh was very different from that of Rh(111) and Pt(111) electrodes, whereas the behavior of the two layer thick film was similar to that of a bulk Rh(111) electrode.

The initial stages of Rh deposition on Au(111) were studied by Kibler *et al*. using *in situ* STM and voltammetry [33]. They characterized the electrocatalytic properties of Rh films with an average thickness of a few layers using CO oxidation as a test reaction. Arbib *et al*. investigated the mechanism of Rh film formation on polycrystalline Au and Au(100) surfaces by voltammetry and chronoamperometry [25]. Their results on Au(100) indicate that two monolayers of Rh could be deposited before the nucleation and growth of 3D Rh clusters. Zou and Weaver overviewed the electro-deposition procedure for preparing ultrathin films of Pt-group metals and their application in surface enhanced Raman scattering (SERS) studies [34]. They pointed out that galvanostatic deposition at low deposition currents leads to the formation of uniform and pinhole-free films. All Rh films in this study were prepared by such a galvanostatic deposition method.

In comparison with the IRRAS technique, which is characterized by the presence of a thin solution layer in the optical path, surface enhanced infrared absorption spectroscopy (SEIRAS) in the internal attenuated total reflection (ATR) configuration [35, 36] provides many advantages for equilibrium and time resolved *in situ* studies at electrochemical interfaces. These advantages are threefold: (1) high and specific surface

sensitivity of the IR response with an enhancement factor up to about 100; (2) dominant first layer effect with a probing range of a few nanometers; (3) no limitation of the mass transport and perturbation of potential distribution. Due to the surface selection rule for SEIRAS [37], only molecular vibrations having dipole changes normal to the local surface are enhanced. This effect allows distinguishing the orientation of adsorbed molecules. Direct access to chemical information on structure and dynamics of the electrode/electrolyte interfaces can be provided by this *in situ* spectroscopic approach, which has been employed as a powerful tool in the investigations of catalytically-active solid/liquid interfaces [38-41]. However, the ATR-SEIRAS technique requires the use of thin film electrodes, which usually have a less ordered surface structure than bulk single crystal electrodes.

In this article, we describe the preparation of thin Rh films on quasi single crystalline Au(111-25 nm) film electrodes and report the first ATR-SEIRAS study of CO adsorption and electro-oxidation on these Rh film electrodes. This study is complemented by IRRAS experiments with Rh(111), Rh(100) and Rh(110) electrodes. The application of structure-sensitive techniques, which address directly the local phenomena at the solid/liquid interface under electrochemical conditions, allowed us to correlate the reactivity and the structure of the Rh electrodes.

2. Experimental

The electrolyte solutions were prepared from Milli-Q water (18 MΩ cm, total organic carbon < 4 ppb), H_2SO_4 (98%, Merck, suprapur) and $RhCl_3 \cdot 5H_2O$ (99.999%, Aldrich). Argon (5N, Carbagas) was used to remove air and CO from solutions. All the

glassware was cleaned by boiling in 25% HNO_3 solution and rinsed thoroughly with Milli-Q water. All the potentials are quoted vs. the reversible hydrogen electrode (RHE). Atomic Force Microscopy (AFM) imaging of the Au and Au/Rh films was carried out in an ambient environment with PicoPlus 5500 SPM system (Agilent Technologies) in contact mode using PPP-CONTR cantilevers (Nanosensors). All measurements were done at room temperature.

Au(111-25nm) film electrodes

The 25 nm thick Au film was prepared on the flat side of a silicon hemisphere by electron beam evaporation as described in Ref. 42. Well-defined Au(111) terraces were produced by electrochemical [43] or flame annealing.

Rh/Au(111-25nm) film electrodes

The Rh films employed in the ATR-SEIRAS experiments were galvanostatically electro-deposited on the surface of the Au(111-25 nm) film from a 5 mM $RhCl_3$ + 0.1 M H_2SO_4 + 0.3 mM HCl plating solution by applying a current density of 32 μA cm^{-2} for 150 s. The deposition was done in the SEIRAS cell that was mounted on top of the gold-covered silicon hemisphere and equipped with a Pt coil counter electrode and a hydrogen-trapped RHE reference electrode. After deposition, the electrolyte was exchanged without exposing the film to the air with deaerated 0.1 M H_2SO_4 solution for 6 times to remove the residue of the plating solution. Then the resulting Rh/Au(111-25 nm) film electrode was electrochemically annealed in the deaerated 0.1 M H_2SO_4 by cycling

the potential between 0.05 V and 0.40 V at 10 or 50 mV s^{-1} for at least 1 h before CO dosing and spectroscopic measurements.

Rh(hkl) single crystal electrodes

The single crystal beads were prepared, oriented, cut and polished as described in Ref. 44. Before each individual experiment, a Rh(hkl) electrode was annealed with a butane burner, then the hot red-colored electrode was transferred to a flask filled with a reductive gas mixture (Ar + H_2 / 90:10), and subsequently cooled down to the room temperature. The electrode was then immersed into deaerated Milli-Q water and transferred to the spectro-electrochemical cell with a protecting droplet of water on the surface. Contact with the electrolyte was typically established under potential control at 0.25 V.

The SEIRAS and IRRAS setups

The SEIRAS measurements were carried out with a Bruker Vertex 80V infrared spectrometer equipped with a liquid-nitrogen-cooled detector (MCT317, Colmar Technologies) using a resolution of 4 cm^{-1}. The spectrometer employed for IRRAS measurements was a Thermo Nexus 8700 also equipped with a MCT detector. The SEIRA spectra were acquired in the so-called Kretschmann attenuated total reflection (ATR) configuration [42]. The IRRA spectra were collected in the external reflection configuration using a spectro-electrochemical cell equipped with a CaF_2 window beveled at 60º. A potentiostat was synchronized with the spectrometer for potential/current control. A non-polarized beam was focused onto the electrode/electrolyte interface by

passing through the modified Si hemisphere in the ATR-SEIRAS experiments whereas a *p*-polarized beam was used for IRRAS measurements. In all cases, the beam incident angle was 60^{o} referred to the electrode surface normal. All the spectra are plotted in absorbance units $A = -\log (R/R_0)$, where R and R_0 represent the intensities of the reflected radiation for the sample and the reference single beam spectra, respectively.

3. Results

3.1 Characterization of Au(111-25 nm) and Rh/Au(111-25 nm) film electrodes

A typical cyclic voltammogram (CV) of Au(111-25 nm) film in 0.1 M H_2SO_4 (Fig. 1) shows well-defined electrochemical features of a (111) oriented single crystal surface, such as the lifting of the (p×√3) reconstruction (P1) and the order/disorder phase transition with the formation/dissolution of (√3×√7) sulfate overlayer (P2/P2'). Two characteristic peaks OA1 and OA2 appeared in the voltammogram during a potential excursion to 1.80 V, which are assigned to the surface oxidation process on steps and on (111) terraces, respectively [45, 46]. In comparison with stepped gold single crystals Au(n,n,n-2) [42], the electrochemical features of the Au(111-25 nm) film (Fig. 1) are similar to those of Au(111) surface with a miscut angle of 2 - 4^{o}, corresponding to (111) terraces with an average width of 19 to 27 atoms. AFM images of Au(111-25 nm) films after the thermal annealing demonstrate large terraces (inset of Fig. 1) with steps intercepting at multiples of 60^{o}, which is characteristic for the (111) surface (Fig. S1c).

The Rh/Au(111-25 nm) film electrodes (inset of Fig. 2A) produced by the electro-deposition of Rh are composed of 3D clusters. This fact complicates the calculation of a Rh coverage value from the charge density passed during the galvanostatic deposition

step. Moreover, if the amount of deposited Rh is too low (low currents and/or low electro-deposition times), the clusters do not cover Au surface completely, as it was demonstrated by the Au-CO bands observed on such samples (see SI). Once the gold surface is almost completely covered by Rh, further Rh deposition leads to the 3D growth of clusters and a further increase of the surface roughness (see detail in SI).

Figure 2A shows a cyclic voltammogram of a Rh modified Au(111-25 nm) film electrode in the deaerated 0.1 M H_2SO_4 recorded at 10 mV s^{-1} in the potential range 0.04 V $\leq E \leq$ 0.70 V. Similar to Rh single crystal electrodes [22], three potential regions labeled I to III can be distinguished: (I) the region of hydrogen adsorption/desorption superimposed by sulfate desorption/adsorption; (II) the electric double layer region; and (III) the region of Rh surface oxidation/reduction. Hydrogen adsorption starts around 0.23 V in the negative-going sweep and produces two overlapping cathodic peaks at 0.10 and 0.09 V (P1), followed by the onset of hydrogen evolution at $E <$ 0.07 V. The corresponding charge density under the cathodic peak was estimated to be ~ 240 μC cm^{-2}.

Figure 2B illustrates a series of selected potential-dependent SEIRA spectra of the Rh/Au(111-25 nm) in 0.1 M H_2SO_4, acquired during a positive potential sweep at 5 mV s^{-1} in the potential range from 0.07 V to 0.95 V. With the increase of potential, the spectra exhibit positive- and negative-going bands indicating, respectively, the accumulation and the depletion of the species in the interfacial region at the sample potential as compared to 0.07 V, where the reference spectrum was acquired. Two pronounced negative-going bands were identified in the spectra at $E >$ 0.09 V, namely a broad band at 3444 ~ 3499 cm^{-1} and a relatively narrow band at ca. 1616 cm^{-1}. They were assigned, respectively, to OH stretching (ν_{OH}) and HOH bending (δ_{HOH}) modes of weakly hydrogen-bonded

interfacial water molecules [47-49]. A positive-going band at ~1118 cm^{-1}, which is attributed to the S-O stretching mode of adsorbed sulfate species (ν_{SO}), appeared at E = 0.15 V [50]. The latter potential value is lower than that reported for the bare Au film surface (0.60 V) [42], indicating stronger adsorption of sulfate on the Rh surface. During the positive sweep, the intensity of all water and sulfate vibration bands increased with the electrode potential up to 0.60 V, indicating a continuous replacement of interfacial water by adsorbed sulfate anions. The band intensity values became constant at E > 0.60 V where surface oxide started to form on the Rh film surface (potential region III).

3.2 CO adsorption on Rh/Au(111-25 nm) film electrodes

CO was adsorbed on the Rh/Au(111-25 nm) film electrode in the 0.1 M H_2SO_4 solution by dosing at 0.10 V for 10 min followed by 20 min purging with Ar in order to remove CO from solution. Figure 3A shows selected time-dependent SEIRA spectra recorded in this experiment, which are referred to a single beam spectrum measured at 0.10 V before CO dosing. Three characteristic CO vibration bands at 2104, 2024 and 1900 cm^{-1} appeared and evolved with time. A small feature at 2104 cm^{-1} is attributed to a CO stretching mode of physisorbed CO on rhodium-free gold sites (ν_{COL}(Au)) (see SI). The 2024 and 1900 cm^{-1} bands correspond to the stretching modes of CO adsorbed on Rh atop (ν_{COL}) and bridge (ν_{COB}) sites, respectively [12, 32, 51]. As mentioned above, the observation of the ν_{COL}(Au) band indicates that the Au(111-25 nm) film surface was not completely covered by the Rh film and there were some free Au sites exposed to the electrolyte solution. The intensity of ν_{COL}(Au) band was much weaker than those for CO on Rh and it disappeared after purging the working solution with Ar (see detail in SI).

Simultaneously with the emergence of the three CO vibration bands, three water bands were observed at 3604, 3500-3050 and 1637 cm^{-1}. They were identified as the OH stretching of isolated interfacial water molecules (ν_{OH1}) [52, 53], the OH stretching of the hydrogen bonded water (ν_{OH2}) and the bending mode of interfacial water (δ_{HOH}), respectively. The band intensities of all the three water bands increased with time during CO adsorption, indicating the coadsorption of water with the CO adlayer, as described by Osawa [54], with one (isolated) OH bond buried in CO adlayer and the other (hydrogen bonded) OH pointing up into solution. Moreover, we stress that they did not disappear after purging with Ar, proving that they are related to CO adsorbed on Rh sites. In addition, a negative-going sulfate band (ν_{SO}) was observed at 1105 cm^{-1}, indicating that a certain amount of sulfate already adsorbed at the Rh/Au(111-25 nm) surface at 0.10 V was replaced by the interfacial CO-water coadsorption structures upon CO dosing.

Figure 3B illustrates the time-dependent evolution of the integrated intensity of the CO stretching bands on Rh, ν_{COL} and ν_{COB}, observed in the spectra reported in Figure 3A. Initially, the CO adsorption started at the bridge site; the occupation of atop sites started after ca. 200 s, when the intensity of ν_{COB} band reached ca. 20% of the maximum value. The band intensity of both ν_{COB} and ν_{COL} reached their maximum and became saturated at 550 s. During the Ar purging ($t > 600$ s), the intensity of the ν_{COL} band was increasing further while that of ν_{COB} was gradually decreasing. The time-dependent partial interconversion from ν_{COB} to ν_{COL} indicate that adsorbed CO molecules moved from the bridge Rh sites to the atop Rh sites of Rh/Au(111-25 nm) surface. Figure 3C shows the time-dependent band frequency plots for ν_{COB} and ν_{COL} bands. Both bands blue-shifted rapidly in the initial period of CO dosing ($t < 360$ s) and then slightly red-shifted during

the following Ar purging process. We attribute the latter to the decrease of the dipole-dipole coupling between CO molecules, which indicates the relaxation of the CO adlayer when CO was removed from the solution.

3.3 CO oxidation on Rh/Au(111-25 nm) film electrodes

After the removal of CO from the solution, we slowly scanned the electrode potential between 0.07 V and 1.10 V at 5 mV s^{-1} (Fig. 4A), while simultaneously recording SEIRA spectra (Fig. 4B). The electro-oxidation of the CO monolayer starts around 0.61 V and displays a single current peak with the main maximum at 0.64 V (CO1). By comparing the charge of CO stripping and that of H adsorption determined from the voltammogram in Figure 4A (see below), we estimated the coverage of CO to be ca. 0.81, which is a value lower than that obtained for a bulk polycrystalline Rh electrode in H_2SO_4 (θ_{CO} = 0.95) [55]. The main CO oxidation peak in Figure 4A is followed by a broad tail up to 1.10 V attributed to the formation of surface oxide on Rh surface (SO). In the subsequent cathodic scan, two distinct peaks were observed at 0.50 and 0.11 V. They are assigned to the reduction of surface oxide (SO') and to the coupled hydrogen adsorption/anion desorption processes (P1), respectively. Judging from the charge under P1 peak, which is similar to that measured before CO dosing, it can be stated that the electro-oxidation of CO adsorbed on the Rh/Au(111-25 nm) film electrode is completed in one anodic potential sweep. This statement will be confirmed by the SEIRA experiments described below. We also note that the overall voltammetric behavior of Rh/Au(111-25 nm) film resembles that of Rh(110) rather than Rh(111) [22, 31].

Figure 4B shows selected potential-dependent SEIRA spectra of CO oxidation on Rh/Au(111-25 nm) electrode with the spectrum acquired at 1.10 V as the reference. Apart from two clearly discerned CO stretching potential-dependent vibration modes at ca. 2020 and 1890 cm^{-1}, the isolated (ν_{OH1}) and the hydrogen bonded (ν_{OH2}) OH stretching modes and the HOH bending mode (δ_{HOH}) of the interfacial water molecules were also observed, together with anion-related negative-going bands around 1126 cm^{-1}. This latter feature corresponds to anions adsorbed at the reference potential just after CO oxidation. All CO bands decrease their intensity with increasing potential, and no CO was left on the surface at 1.10 V where the reference spectrum was acquired.

Figure 5A shows the potential-dependent intensity change of the CO vibration modes on Rh film, ν_{COL} and ν_{COB}, during the first anodic potential scan of the spectra reported in Figure 4B. The peak intensity of ν_{COL} increases with potential, while that of ν_{COB} decreases gradually before reaching the onset of the CO oxidation. According to the voltammetric curves reported in Figure 4A, no CO electro-oxidation occurs in the potential range $E < 0.61$ V. Therefore we interpret these results as the consequence of the interconversion of CO adsorption sites by moving from bridge to atop sites. In other words, the band interconversion during the anodic potential scan suggests that there is a potential-dependent preference of CO adsorption sites on Rh surfaces. At more positive potentials, first the intensity of the ν_{COL} band starts to decrease at $E \geq 0.61$ V, which is followed by a sharp intensity decrease of ν_{COB} band at $E \geq 0.65$ V. The decrease of the ν_{COL} band coincides with the onset of the electrochemical CO oxidation on the Rh film surface as observed in the corresponding CV (Fig. 4A) as well as with the detection of CO_2 bands in the IRRAS experiments (see SI). Therefore, considering the relatively low

surface mobility of adsorbed CO on Rh surface, we conclude that the CO oxidation starts from CO that is adsorbed in atop configurations.

Figure 5C shows that the integrated intensity of the interfacial water band (ν_{OH1}) observed in Figure 4B remains almost constant before the onset of the CO oxidation and starts to decrease at ~0.60 V, which coincides with the decrease of ν_{COL} band intensity. This suggests that the co-adsorbed isolated interfacial water is either actively involved in the initial stage of the CO oxidation process or acts as a probe of local CO coverage, as proposed by Stimming et at. for CO adsorption and oxidation on Pt electrode [56]. Such behavior of water bands has been also reported on Pt [57, 58], Pd [59, 60], Ru [61] and PtRu [62].

The potential-dependent evolution of CO stretching band positions (Fig. 5B) shows that the band frequencies for both ν_{COL} and ν_{COB} bands shifted to higher frequency before the onset of the CO oxidation. The Stark tuning rate for ν_{COL} is around 42 $cm^{-1} V^{-1}$, while for ν_{COB} it slightly changed from 29 to 37 $cm^{-1} V^{-1}$ at ca 0.35 V. The band frequencies for both atop and bridge-bonded CO suddenly decreased after the onset potential of the CO oxidation (0.61 V). It is interesting that the band positions of the isolated interfacial water also changed with potential up to ca. 1.00 V (Fig. 5D), with the Stark tuning rate for $E <$ 0.60 V equal to 43 $cm^{-1}V^{-1}$, while they remain almost constant on the Pt surface [63].

3.4 CO oxidation on Rh(111) electrode monitored with IRRAS

In order to facilitate interpretation of the SEIRA spectra, complementary IRRAS studies of CO oxidation on the three low-index Rh single crystal surfaces were carried out. Figure 6A shows typical cyclic voltammograms of CO stripping from Rh(111) in 0.1

M H_2SO_4 electrolyte solution. Firstly, CO was dosed at 0.25 V for 5 min to form a saturated CO adlayer on Rh(111) surface in the hanging meniscus configuration. Then CO was completely removed from the bulk of solution by gently purging Ar through the electrolyte. Subsequently, the electrode potential was scanned with the rate of 2 mV s^{-1}. The solid line represents the first scan of CO oxidation, while the second scan is indicated by the dotted lines. Adsorbed CO blocks completely the hydrogen/anion adsorption/ desorption features appearing at 0.15 V on the CO-free surface. The onset potential of the main CO oxidation peak is 0.58 V, where the current started to increase, generating a sharp CO oxidation peak with a maximum at 0.63 V (CO1) followed by a pronounced tail in the descending branch. This broad feature has a shoulder peak around 0.78 V, which is superimposed with the oxidation peak of Rh surface around 0.86 V (SO). In the subsequent negative potential scan, two features at 0.71 and 0.57 V were observed. The peak at 0.71 V is attributed to the reduction of the Rh(111) surface oxide (SO'). Appearance of peaks corresponding to the hydrogen adsorption/anion desorption (P1) at 0.11 V with a charge density lower than that observed before CO dosing indicate that the CO is still present on Rh(111) after the first potential scan at 2 mV s^{-1}. In fact, second potential cycle still shows CO oxidation onset at 0.55 V followed by the peak with a maximum at 0.63 V. This behaviour is in a good agreement with the values previously reported from the CV recorded at 1 mV s^{-1}, although decreasing scan rate causes a slight negative shift of the CO oxidation main peak and Rh surface oxidation peak [22].

In an experiment parallel to that reporting in Figure 6A, the IRRAS spectra were recorded during a potential sweep between 0.10 V and 0.90 V at 2 mV s^{-1}. Figure 6B shows the potential-dependent IRRAS response for the first anodic scan of CO oxidation

on Rh(111) electrode in 0.1 M H_2SO_4. The spectrum acquired at 0.10 V after complete removal of CO from Rh surface was chosen as the reference. In Figure 6B, two positive-going bands are specified at 0.10 V, the one at 2029 cm^{-1} is attributed to CO bound to atop sites (ν_{COL}) and the one at lower frequency 1797 cm^{-1} is attributed to multi-fold bonded CO on Rh sites (ν_{COM}) [9, 12, 32, 64]. Atop CO stretching band exists in the entire potential region from 0.10 V to 0.90 V while the multi-fold CO band disappears at potentials around 0.79 V, which is consistent with observations in Refs. 9 and 12.

A detailed potential-dependent evolution of both band frequencies and intensities for the first oxidation cycle are plotted in Figure 7. An obvious blue shift of the band frequency of both ν_{COL} and ν_{COM} vibration modes was observed with the increase of potential up to ca. 0.66 V, for which Fig. 7A shows that both the integrated intensities of ν_{COL} and ν_{COM} remain almost constant. The respective Stark tuning rate values are 27 cm^{-1} V^{-1} (up to 0.66V) and 63 cm^{-1} V^{-1} (up to 0.34 V), respectively. The ν_{COM} tuning slope value slightly decreases to 35 cm^{-1} V^{-1} for potentials between 0.34 and 0.65 V. The band intensities of the ν_{COM} and ν_{COL} modes start to decrease at 0.64 V. However, whereas the ν_{COM} band goes down to nil at $E > 0.79$ V, there is still a high band intensity of ν_{COL} even at $E = 0.90$ V. The peak position of the ν_{COL} shift to lower frequencies at potentials between 0.64 and 0.73 V, then subsequently start to increase again with a Stark tuning rate of 42 cm^{-1} V^{-1} at $0.73 \leq E \leq 0.90$ V.

In the subsequent negative-going potential scan after the collection of the spectra in Figure 6B, only the ν_{COL} band was observed at 0.90 V (see Fig. S6B). The peak positions of ν_{COL} shift to lower frequencies with decreasing potentials with a Stark tuning rate of 42 cm^{-1} V^{-1} (Fig. 8A), same as that at the end of the previous cathodic cycle (Fig. 7B). The

slope then increases to 230 cm^{-1} V^{-1} at 0.47 V followed by the decrease in the band intensity down to 0 at 0.25 V (Fig. 8B). At E = 0.52 V, a new band appears at ca. 1845 cm^{-1} shifting up to 1890 cm^{-1} at 0.30 V and decreasing down to 1825 cm^{-1} at 0.10 V (see Figures S6B and 8). The band position of the peaks is higher than ν_{COM} but lower than ν_{COL}, and they are attributed to a bridge-bonded CO on Rh surfaces (ν_{COB}) [15, 32]. The multi-fold CO signal ν_{COM} was not detected in the negative going scan.

In the second anodic potential scan, only the ν_{COB} band was observed at 0.10 V. At potentials around 0.40 V, ν_{COL} reappears after the disappearance of ν_{COB} band (Fig. S6C). Thus, only ν_{COL} band appears at the start of the second cathodic scan at 0.90 V and with a band intensities decreasing in parallel to the appearance of the ν_{COB} band at lower potentials (Fig. S6D). The coverage of CO decreased with each potential cycle, and thus the peak intensity also decreased. The observation of this potential-dependent interconversion of adsorption site from ν_{COL} to ν_{COB} or vice versa provides clear evidence that there is an effect of the electrode potential on the preferred CO adsorption sites on Rh(111).

It is interesting to note that the potential-dependent IRRA spectra for the CO oxidation process on Rh(110) and Rh(100) surfaces show only one CO vibration mode; ν_{COL} around 2010 cm^{-1} on Rh(110) and ν_{COB} around 1930 cm^{-1} on Rh(100), respectively (see detail in Fig. S7). No CO stretching mode due to the multi-fold bonded CO (ν_{COM}) was observed on these two low-index Rh surfaces. On the other hand, Weaver *et al*. observed both ν_{COL} and ν_{COB} bands during CO oxidation on both Rh(110) and Rh(100) surfaces [11, 12]. The discrepancies with results reported here might be caused by the different surface quality of the Rh electrodes used. In their study, the Rh electrodes were

prepared by a more complicated method which may bring in some unexpected defects resulting CO adsorbed on different defect sites. When comparing the spectra obtained in different laboratories, the effect of carbon monoxide coverage on the type and frequencies of the CO bands (related in some experiments to the absence/presence of CO in solution) has to be taken also into account. In our data, the intensities of CO bands for Rh(110) and Rh(100) electrodes almost remain constant until 0.47 V. Then there is almost no CO left at $E > 0.60$ V. The peak positions of ν_{COL} on Rh(110) and ν_{COB} on Rh(100) show a clear blue shift trend before the onset of CO oxidation with a Stark tuning rate of 37 cm^{-1} V^{-1} and 15 cm^{-1} V^{-1}, respectively.

4. Discussion

4.1. Properties of Rh film on Au(111-25 nm) film electrode

The Au films prepared on Si prism has a preferential (111) surface structure as deduced from their electrochemical behavior and the corresponding AFM images. Despite a high degree of surface order, the resulting Au(111-25 nm) films still exhibit a high enhancement of infrared absorption for adsorbates (SEIRAS effect). In this study, a Rh thin film was deposited electrochemically on the Au(111-25 nm) film by applying a constant current in a Rh-containing plating solution. The thickness of the Rh film obtained with this galvanostatic electro-deposition method was controlled by the electro-deposition time as well as by the concentration of the $RhCl_3$ in the plating solution. After the optimization of the experimental conditions (see detail in SI), we found that a deposition time of 150 s in a 5 mM $RhCl_3$ produces Rh thin films with a formal thickness of a few monolayers as calculated by employing a method of Kibler *et al*. [33]. It is very

difficult to estimate how much of gold surface is actually covered by Rh because its electro-deposition follows a nucleation and growth mechanism leading to the formation of 3D cluster structures. This behavior is in a strong contrast with the epitaxial growth of Rh on Pt single crystal surfaces [30-32]. In the cyclic voltammogram for the Rh/Au(111-25 nm) films in 0.1 M H_2SO_4 (Fig. 2A), the charge density under the hydrogen adsorption peaks was calculated to be ~240 μC cm^{-2}. This charge density value is higher than that measured for a Rh(110) electrode (Q_{Had}: 160 μC cm^{-2}), but significantly lower than that for Rh(111) (Q_{Had}: 360 μC cm^{-2}) [22].

In addition to the charge for the hydrogen adsorption/desorption in CV, information on the surface structure of the Rh films can be obtained from the comparison of the voltammetric profiles for the carbon monoxide stripping process. In our previous work, detailed electrochemical properties of low-index Rh single crystal surfaces have been determined in 0.1 M H_2SO_4 in the absence and in the presence of CO on the Rh surface [22]. The CO coverages on Rh(hkl) electrodes were estimated using the net charge density of CO stripping combined with hydrogen and anion adsorption [31, 65]. Values obtained for Rh(111), Rh(110) and Rh(100) were found to be 0.75, 0.98 and 0.92, respectively. The CO coverage on Rh(111) is approximately 20 % lower than on other two surfaces, these two latter values being similar to that reported on a polycrystalline surface (θ_{CO} = 0.95) [55]. The CO coverage value for the Rh films prepared in this work was calculated to be 0.81 (Fig. 4A), indicating again a notable contribution of Rh(111) sites in the current Rh film surface. However, the shape of the voltammetric profile for the Rh films (Fig. 2A) resembles that on the Rh(110). Finally, the presence of defects at the surface of the Rh film electrodes is witnessed by the faster electro-oxidation of

adsorbed CO, which, in contrast to the behavior of well-ordered Rh(111) electrodes, takes place in a single potential excursion up to 1.10 V.

Further information on the surface structure of the Rh thin films prepared in this work can be indirectly derived from the comparison of their infrared spectra for adsorbed CO with those obtained for Rh single crystal electrodes. The SEIRAS study of CO adsorption on the Rh/Au(111-25 nm) film shows the existence of two distinctive CO stretching bands corresponding to different adsorption configuration: atop CO and bridging CO. The IRRA spectra obtained for CO adsorbed on Rh electrodes with the three low-index orientations show one or two different CO stretching bands corresponding to different combinations of adsorption sites depending on the surface orientation, the CO coverage and the electrode potential. Regarding the Rh(100) and Rh(110) electrodes, they showed only signals corresponding to a single type of adsorbed CO: atop CO on Rh(110) and bridge CO on Rh(100), respectively. In the case of the Rh(111) electrode, atop and multi-fold adsorbed CO are observed for the saturated CO adlayer, whereas atop and bridge sites are occupied after partial CO oxidative stripping. Note that multi-bonded CO_M has been observed only on a well-defined Rh(111) surface [9, 12, 32, 66], indicating that CO_M is preferentially formed on well-ordered Rh(111) terrace sites. In this way, it can be recalled that a potential excursion up to 0.90 V with the Rh(111) electrode leads to the formation of surface oxide, which could drastically change the surface morphology of well-ordered Rh(111) terrace site after the reduction of surface oxides.

These changes in the surface structure of the Rh(111) electrode could be at the origin of the emergence of the CO_B band instead of CO_M band in the subsequent cathodic scan

after the surface oxidation. This interpretation would be consistent with the hypothesis of the preferential formation of CO_M only on the well-ordered Rh(111) terrace sites. However, the decrease in the CO coverage upon partial oxidation of the CO adlayer can also be invoked to justify the absence of multi-bonded CO. In any case, the existence of two kind of adsorbed CO as well as the observation of the potential-dependent interconversion of CO adsorption configuration (see below) can be considered as characteristics of (111) adsorption sites. Therefore, the Rh films prepared in this study show electrochemical properties of Rh(110) simultaneously with spectroscopic features of Rh(111) terrace. The latter would not be wide enough to accommodate the CO adlayer containing multi-bonded CO. Presumably the resulting Rh film surface has a highly stepped [n(111) × (111)]-like surfaces with a preferential (111) narrow terraces.

4.2. Interconversion of adsorbed CO configuration

Another piece of spectroscopic information related to the presence of (111) sites in the Rh thin film electrodes is the interconversion of adsorption configuration between CO adsorption sites, which has been observed in this work under a variety of experimental conditions. The existence of a potential-dependent band interconversion between atop CO (CO_L) and multi-fold CO (CO_M or CO_B) has been clearly demonstrated from the analysis of the IRRA spectra obtained during the CO oxidation process on Rh(111). Fully CO-covered Rh(111) shows two CO stretching bands (CO_L and CO_M) during the first anodic oxidation scan. The latter adsorption mode disappeared first at $E < 0.79$ V while CO_L remains even when surface oxide starts to form at 0.90 V. The potential-dependent band interconversion was discerned clearly in the subsequent first cathodic scan as a

consequence of the decrease in CO coverage. When we kept the higher limit in the following potential scans in a range below the onset of CO oxidation (ca. 0.60 V), the reversible potential-dependent band interconversion between CO_L and CO_B was observed around 0.45 V for multiple cycles without losing CO from the surface.

Potential-dependent interconversion processes have been observed and reported previously for adsorbed CO [9, 12, 15]. We have already mentioned here the results of the combined *in situ* STM and IRRAS study of CO adsorbed on Rh(111) surface by Yau *et al*. [15]. They showed the existence of two distinctly different CO adlayer structures depending on the electrode potential in a CO-saturated 0.1 M $NaClO_4$ solution. At lower potential, where hydrogen adsorption takes place on the CO-free Rh surface, a $(3\times\sqrt{3})$-4CO structure with a CO coverage of 0.67 was imaged by STM indicating the predominant presence of CO on a bridge site with only one CO_L molecule per unit cell. On the other hand, at higher potentials just below the onset of CO oxidation, a (2×2)-3CO adlayer was observed. The latter CO adlayer corresponds to a CO coverage of 0.75 and includes two CO_L with one CO_B in its unit cell. This structural change in CO adlayer, as discerned by *in situ* STM, correlates well with the substantial variation in spectral features, such as band interconversion, observed here in the IR spectroscopic studies.

In our SEIRA spectra for the Rh thin film electrodes, only atop and bridge CO could be discerned during CO adsorption process at 0.10 V. Partial band interconversion from CO_B to CO_L is observed during the subsequent Ar purging process at 0.10 V. This band interconversion process (Fig. 3B) is probably related to the existence of a surface relaxation process inside the CO adlayer induced by the removal of CO from the bulk solution. Moreover, the potential-dependent intensity change, shown in Figure 5A for the

CO vibration modes on Rh film at around 2020 cm^{-1} (ν_{COL}) and 1900 cm^{-1} (ν_{COB}), just before the onset of CO oxidation reaction during a first anodic potential scan, can be interpreted as a result of the interconversion of CO adsorption sites by moving from bridge to atop sites. This behavior is comparable to that discussed above for the partially CO-covered Rh(111) electrode and supports the existence of (111) domains at the surface of the Rh thin film electrode.

Finally, we recall that the preference of CO adsorption at higher coordinated sites at low potentials is related to an increasing extent of *d*-π* back-donation during the increase of the negative surface charge density. This behavior was predicted by Anderson and Awad [67] on the basis of a molecular orbital calculation. In addition, the potential dependence of the CO stretching frequency could also be determined by the vibrational Stark effect associated to changes of the electric field in the electrical double layer [68, 69]. It is reasonable to imagine that the potential dependence of the binding site preference and the vibrational frequency of adsorbates on electrodes are influenced by a cooperative effect of both factors [68]: the *d*-π* back-donation and the electric field.

4.3. Reaction mechanism of CO oxidation on Rh surfaces

In this section, we will discuss the mechanism of the CO oxidation on Rh surfaces that are discerned from our data. We point out first that infrared spectroscopy provides information on the preference of coordination sites for CO adsorption on Rh surfaces, such as atop, bridging and multi-fold sites. However, it is difficult to discriminate the adsorption site (terraces and defect/step sites) of CO on Rh surfaces only from the

infrared spectra. Therefore, we draw a picture of the reaction mechanism assuming that the defect/step sites are the reactive sites as opposed to inactive terrace sites.

A series of potential-dependent SEIRA spectra collected during CO oxidation on Rh/Au(111-25 nm) (Fig. 4B) shows that the intensity of the CO_L band start to decrease first at the onset potential of CO oxidation as detected in the corresponding voltammograms (Figs. 4A). This observation suggests that CO_L is more reactive than CO_B on Rh surfaces.

Prior to the onset of CO oxidation, it is clearly observed in Figure 5B that the Stark tuning slope value of CO_B at the Rh thin film electrode changed at ~0.34 V. A similar behavior is observed in Figure 7C for CO_M at the Rh(111) electrode. As mentioned above, the Stark tuning slope value may be related both to the strength of the electric field in the double layer and the potential-dependent charge transfer from the electrode to the adsorbed CO molecule, which depends on several environmental conditions at the solid/liquid interfaces, including the coverage of adsorbates, adsorption configuration and vibration modes. Therefore, the change of the Stark tuning slope value at 0.34 V observed in Figures 5B and 7C could be triggered by the change of the adjacent local environment of multi-fold/bridging CO molecules. In other words, the interconversion of adsorption sites between CO_L and CO_B on the Rh electrodes observed at the potential range between 0.34 and 0.40 V causes significant variation in the environmental condition of CO adlayer, and as a consequence, changing the Stark tuning slope value of $CO_{M/B}$. In this way, we propose that the CO oxidation on Rh(111) and Rh thin film surfaces is preceded by the change of adsorption preference of CO from multi-fold sites

to atop sites, which take place in a potential range 0.20 V more negative than the actual onset of CO oxidation.

Moreover, the interconversion of adsorption configuration of CO on Rh may also induce a surface relaxation of CO adlayer, which would provide free surface sites for the dissociative adsorption of interfacial water, leading to the formation of oxygen species, such as OH_{ad}, at defect sites. SEIRA spectra show the simultaneous decrease in the band intensity of ν_{CO} together with the isolated water ν_{OH}, providing direct evidence that the isolated interfacial water molecules are actively involved in the CO oxidation process at the surface.

In consequence, our results on the potential-dependent evolution of adsorbed CO and interfacial water bands suggest the existence of a "reactant pair" mechanism for the reaction between CO_{ad} and OH_{ad} adsorbed on adjacent sites which form CO_2, best described by a Langmuir-Hinshelwood type mechanism [70]. In other words, the CO oxidation reaction takes place only at the interface between two reacting phases (CO_{ad} and OH_{ad}). Since it is generally accepted that the dissociative adsorption of water molecules to form adsorbed OH is faster at the steps than on the terraces, it can be stated that the CO oxidation reaction starts at the step site and then propagate over the terrace site [18, 71]. However, due to the slow mobility of CO molecules on Rh surface [18, 22], instead of the surface diffusion of CO on terrace to step sites as observed on Pt surfaces, the remaining CO on terraces may be distributed as islands, and the oxidation reaction occurs along the periphery of those islands until all adsorbed CO are oxidized by the adjacent OH species. Therefore, initially the reaction is kinetically controlled by the nucleation of OH next to CO.

Stripping of the CO adlayer on Rh(111) surface requires multiple potential cycles, even at such low potential sweep rate as 1 mVs^{-1} [22], due both to the low surface mobility of CO and to the smaller amounts of OH on Rh(111) terrace sites produced by the dissociation of interfacial water. In addition, the sulfate adsorption competes with OH adsorption for the free adsorption sites on Rh surface [17, 18], which can only be produced by the oxidation of CO. The band intensity of CO_L stops decreasing at 0.78 V during the first oxidation cycle, and remains constant at higher electrode potentials (Fig. 7A). At the same time, the band frequency of CO_L increases linearly with potentials with a Stark tuning rate of 42 $cm^{-1}V^{-1}$ (Fig. 7B) at $E > 0.78$ V. These spectroscopic features demonstrate that the CO coverage no longer changes at potentials higher than 0.78 V, thus indicating an interruption of CO oxidation. According to the observed voltammetric behavior, the surface oxide formation on the Rh(111) electrode surface starts at 0.70 V and the corresponding reduction peak in the cathodic scan is observed at 0.71 V (Fig. 6A). As CO oxidation follows a Langmuir-Hinshelwood type reaction mechanism, it is necessary to have adjacent OH_{ad} to oxidize CO. In other words, due to the lack of adjacent OH_{ad} on the Rh surface at high potential due to the further oxidation of OH to surface oxide, CO oxidation is inhibited and CO is left unoxidized on the Rh(111) surface. We therefore propose that the inhibition of CO oxidation is due to the formation of surface oxide rather than due to the competitive adsorption of anions.

In the case of the Rh/Au(111-25 nm) film electrode, we propose that the CO oxidation takes place following a similar reaction mechanism as that proposed for the Rh(111) surface, *i.e.* the Langmuir-Hinshelwood type mechanism. CO oxidation on the Rh film electrode is preceded by the interconversion of CO adsorption site from bridge to

atop configuration at E > 0.34 V. Then the onset of CO oxidation at 0.61 V (Fig. 4A), with a peak maximum at 0.64 V, is followed by a pronounced tail at higher potentials in the anodic scan. The latter tailing part indicates a slow process, controlled by the kinetic of a reaction such as OH_{ad} formation on terrace sites, as well as by a significantly low mobility of CO on terrace sites, which is attributed to the competitive adsorption of strong anion on Rh surface [18]. Due to a higher step density on the Rh film than on Rh(111) (see detail in SI), CO oxidation continues even in the high potential range (E > 0.79 V) and CO oxidation is completed in the first anodic potential scan to 1.10 V.

5. Conclusion

In this study we have prepared Rh-modified Au(111-25 nm) electrodes by a combination of electron beam evaporation and galvanostatic electro-deposition methods for gold and rhodium, respectively. The Rh modified Au film electrodes have been characterized by cyclic voltammetry, AFM and *in situ* SEIRAS, and their behavior compared with that of bare Au(111-25 nm) and low-index Rh single crystal electrodes. It was demonstrated that rough Rh films consisting of 3D clusters were formed on the Au(111-25 nm) film electrode.

ATR-SEIRAS, a direct spectroscopic technique to study various processes at the solid/liquid interfaces, has been employed to characterize the adsorption and electro-oxidation of CO on Rh modified Au(111-25 nm) film electrodes in 0.1 M H_2SO_4. It has been shown that CO adsorbs on Rh film electrode in both atop and bridging configurations. The Rh/Au(111-25 nm) film has a considerable contribution of (111) sites

to the observed spectra, while its electrochemical properties are dominantly attributed to the presence of (110) defect/step site.

The interconversion process between ν_{COL} and $\nu_{COB(M)}$ was clearly demonstrated in the SEIRAS and IRRAS studies and is most probably due to the slow surface mobility of CO on Rh surfaces compared to Pt surfaces. A detailed interpretation of the interconversion process and its kinetics requires additional electrochemical and spectroscopic investigations, such as potential step chronoamperometric experiments and isotopic exchange studies using $^{13}CO/^{12}CO$ gas, which are currently under way.

Finally the reaction mechanism of adsorption and oxidation of CO on the Rh surface in sulfuric acid is discussed on the basis of our electrochemical and SEIRAS data. They confirmed that isolated interfacial water molecules are coadsorbed with CO_{ad}, the former species being dissociated to form adsorbed OH via nucleation at "special" sites, usually defects or steps. Therefore our SEIRAS data supports the "nucleation-and-growth model" of Langmuir-Hinshelwood type reaction proposed for CO oxidation on Rh surfaces in acidic media. The CO oxidation at the Rh surface is characterized by (1) a low surface mobility of CO, (2) a potential dependent interconversion of adsorption sites between atop and bridge positions, (3) propagation of OH_{ad} from step sites into the terrace. These contributions control the overall reaction kinetics of CO oxidation on Rh surfaces.

Acknowledgement

The work was supported by the Research Center Jülich, the University of Bern, the Swiss National Science Foundation (200020_144471, 200021-124643), the Spanish Ministerio de Economía y Competitividad (project CTQ2013-44083-P) and University of Alicante.

QX acknowledges fellowships of the Research Center Jülich; IP acknowledges support by COST Action TD 1002; and AK acknowledges the financial support by CTI Swiss Competence Centers for Energy Research (SCCER Heat and Electricity Storage).

Figure Caption

Figure 1: (A) Steady state cyclic voltammograms of a Au(111-25 nm) film electrode in 0.1 M H_2SO_4, scan rate: 10 mVs^{-1} (black line) and magnified (× 25) CV of double layer region (red line). Inset: AFM image of Au film surface after flame annealing: Image size 150 × 150 nm, height scale 4 nm.

Figure 2: (A) CV at 10 mVs^{-1} in 0.1 M H_2SO_4 and an AFM image (inset) of Rh/Au(111-25 nm) film: image size 1 × 1 μm; (B) Selected SEIRA spectra of Rh/Au(111-25 nm) in 0.1 M H_2SO_4 as a function of potential; the reference spectrum was recorded at 0.07 V.

Figure 3: (A) Selected time-dependent SEIRA spectra obtained during CO dosing (0-600 s) and subsequent Ar purging (600-1800 s) on Rh/Au(111-25 nm) in 0.1 M H_2SO_4 at 0.10 V. Time-dependent evolution of the integrated intensities (B) and band positions (C) of CO stretching modes (ν_{COL}) and (ν_{COB}). The reference spectrum was recorded at 0.10 V before CO dosing. The dashed line in (B) and (C) indicates the time when Ar purging was initiated to remove CO from the electrolyte solution.

Figure 4: (A) CV of CO stripping and (B) potential-dependent SEIRA spectra recorded at 5 mV s^{-1} in a CO-free 0.1 M H_2SO_4 solution during the electro-oxidation of CO adlayer deposited at 0.10 V on Rh/Au(111-25 nm). The reference spectrum in (B) was recorded at 1.10 V.

Figure 5: Potential-dependent evolution of the integrated intensities (A,C) and band positions (B,D) of CO stretching modes (ν_{COL} and ν_{COB}) (A,B) and OH stretching (ν_{OH1}) (C,D) during CO oxidation. See caption of Fig. 4 and text for further details.

Figure 6: (A) CV and (B) potential-dependent IRRA spectra recorded in CO-free 0.1 M H_2SO_4 during potential scan at 2 mV s^{-1} during the electro-oxidation of CO adlayer deposited at 0.10 V on Rh(111). The reference spectrum in (B) was recorded at 0.10 V in the absence of CO on the surface.

Figure 7: Potential-dependent evolution of the integrated intensities (A) and band positions (B,C) of CO stretching modes ν_{COL} and ν_{COM} during the 1st anodic scan for the CO oxidation. See caption of Fig. 6 and text for further details.

Figure 8: Potential-dependent evolution of the band positions (A) and the integrated intensities (B) of CO stretching modes ν_{COL} and ν_{COB} during the 1st cathodic scan for the CO oxidation. See caption of Fig. 6 for further details.

Figure 1

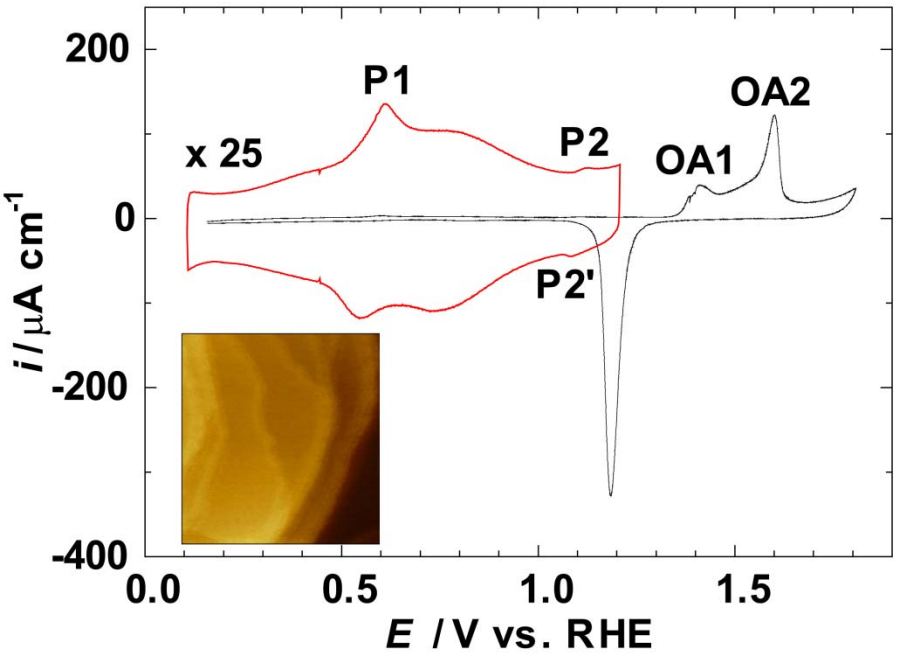

Figure 2

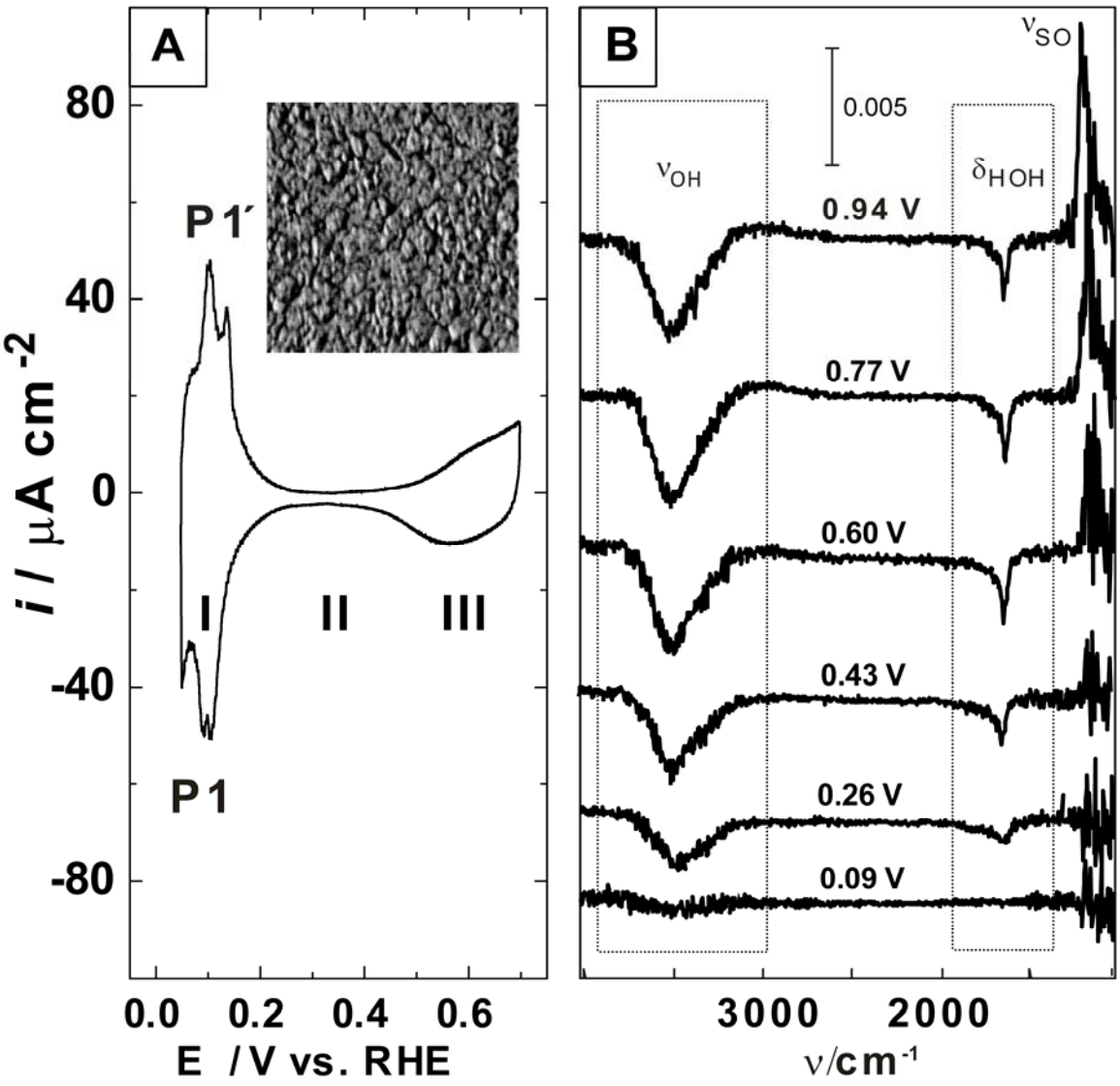
A
B
80
40
0
-40
-80
i / μA cm-2
P1´
P1
I
II
III
0.0
0.2
0.4
0.6
E /V vs. RHE
νSO
0.005
νOH
δHOH
0.94 V
0.77 V
0.60 V
0.43 V
0.26 V
0.09 V
3000
2000
ν/cm-1

Figure 3

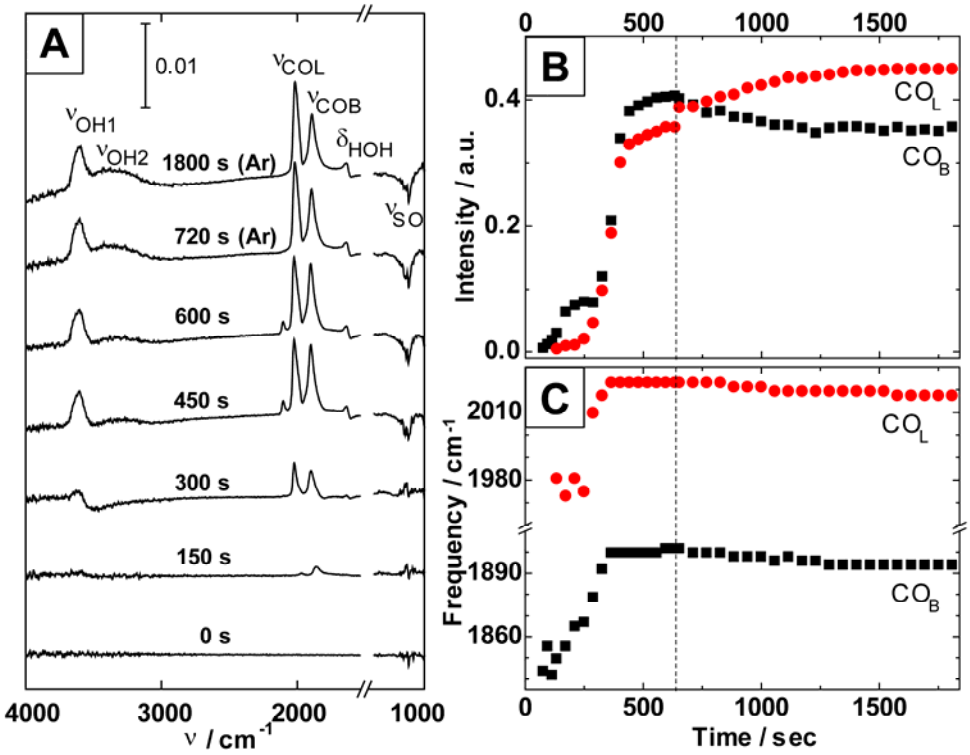
A
0.01
ν_{COL}
ν_{COB}
δ_{HOH}
ν_{OH1}
ν_{OH2}
1800 s (Ar)
720 s (Ar)
600 s
450 s
300 s
150 s
0 s
ν_{SO}
4000
3000
2000
1000
ν / cm^{-1}
B
C
Intensity / a.u.
Frequency / cm^{-1}
CO_L
CO_B
0
500
1000
1500
Time / sec

Figure 4

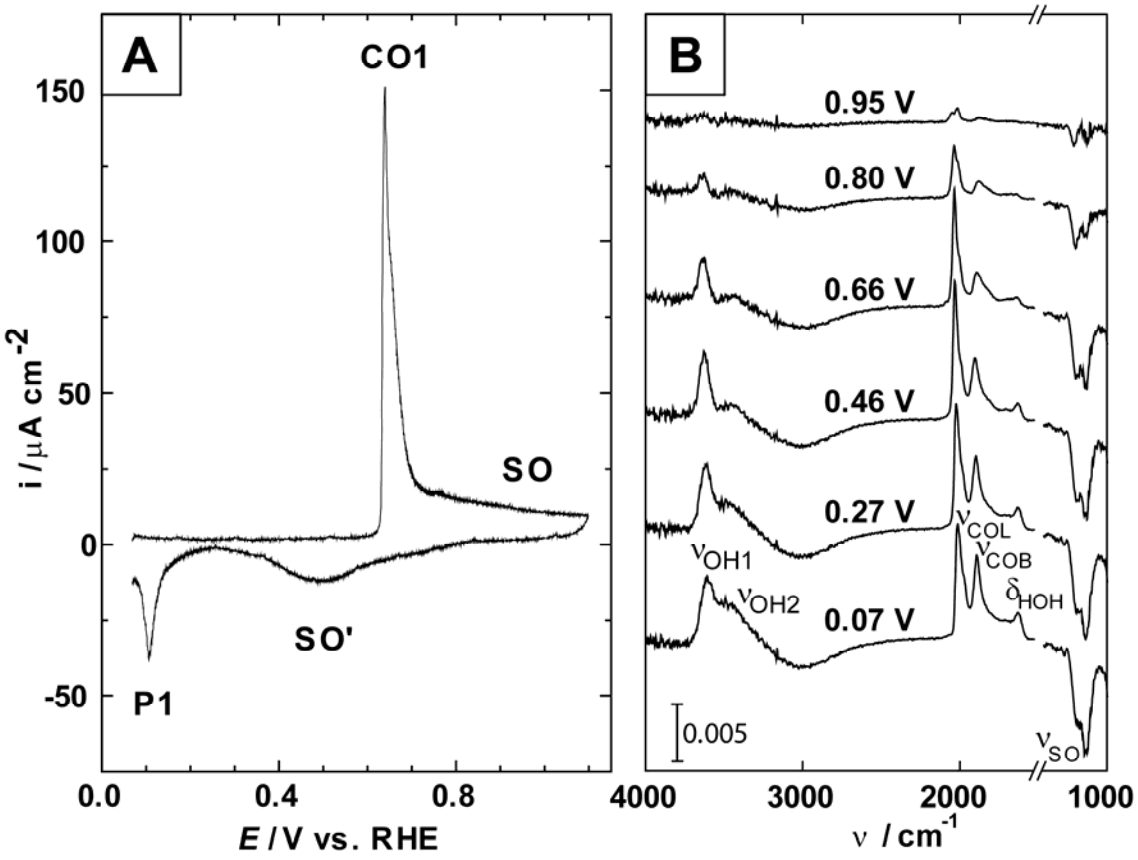
A
CO1
SO
SO'
P1
150
100
50
0
-50
i /μA cm-2
0.0
0.4
0.8
E / V vs. RHE
B
0.95 V
0.80 V
0.66 V
0.46 V
0.27 V
0.07 V
νOH1
νOH2
νCOL
νCOB
δHOH
νSO
0.005
4000
3000
2000
1000
ν / cm-1

Figure 5

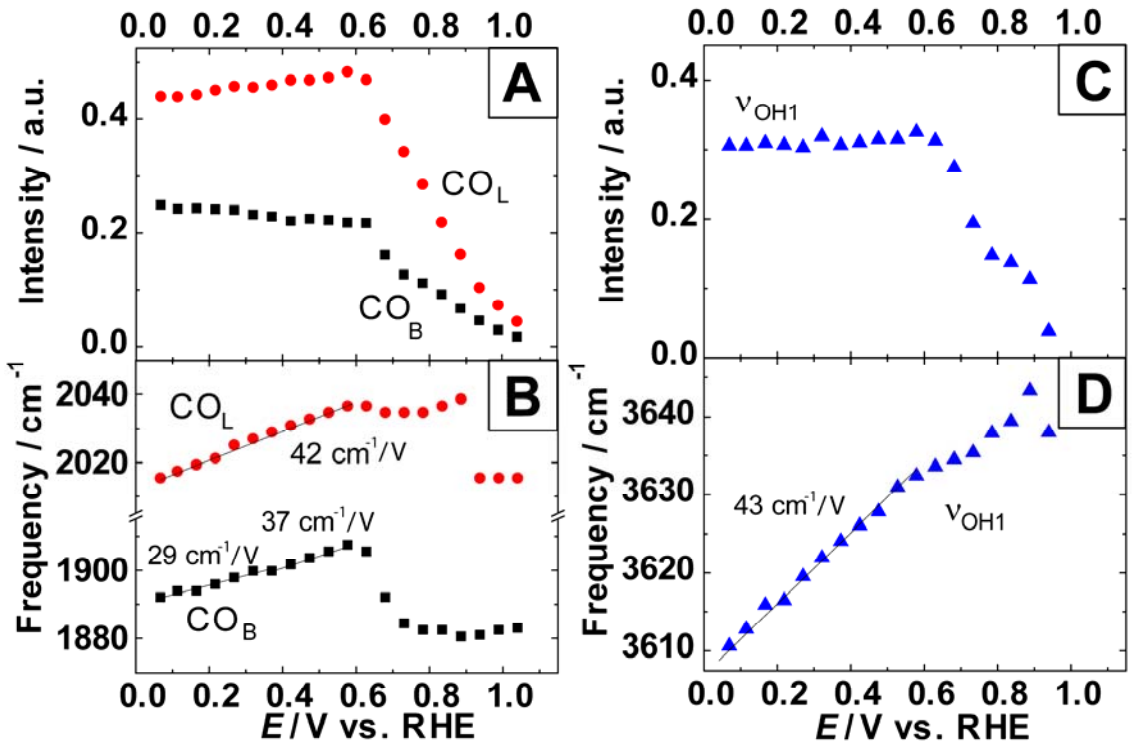
A
B
C
D
Intensity / a.u.
Frequency / cm-1
E / V vs. RHE
CO_L
CO_B
42 cm-1/V
37 cm-1/V
29 cm-1/V
ν_OH1
43 cm-1/V

Figure 6

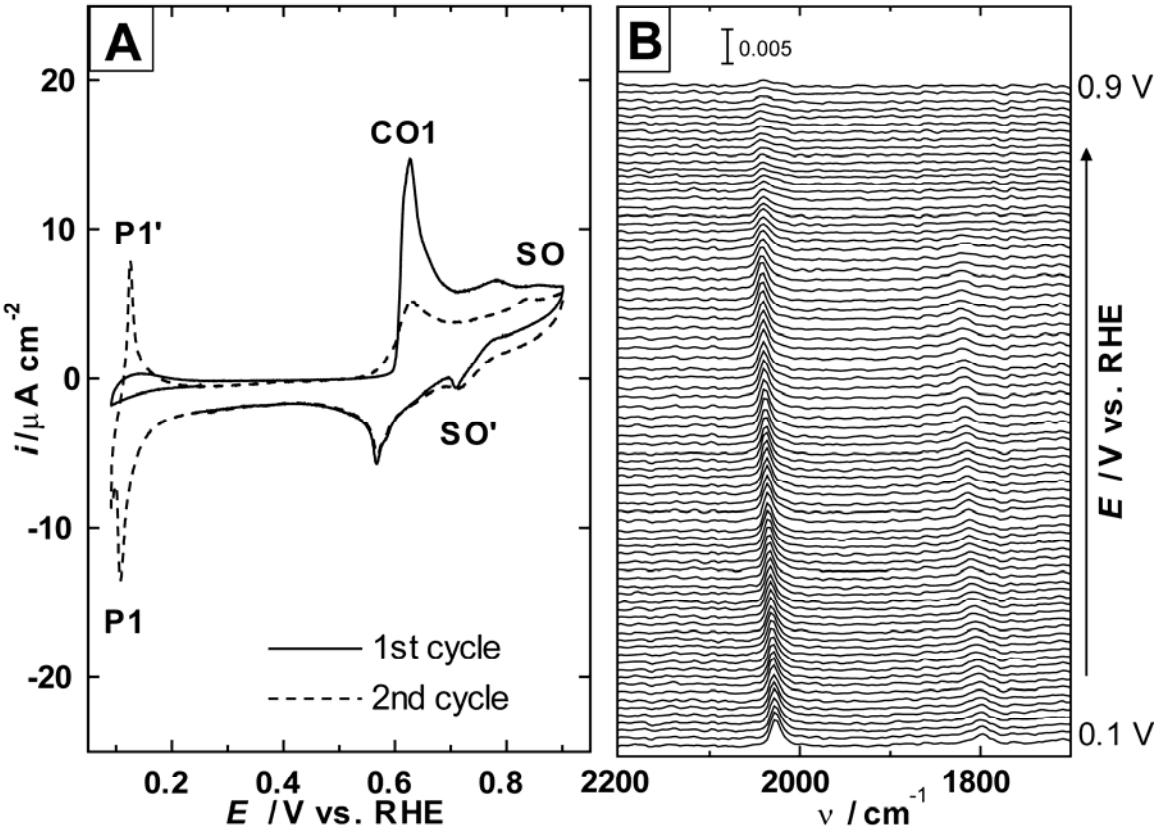
A
B
0.005
CO1
P1'
SO
SO'
P1
1st cycle
2nd cycle
i/μA cm-2
E /V vs. RHE
ν /cm-1
0.9 V
0.1 V
E /V vs. RHE

Figure 7

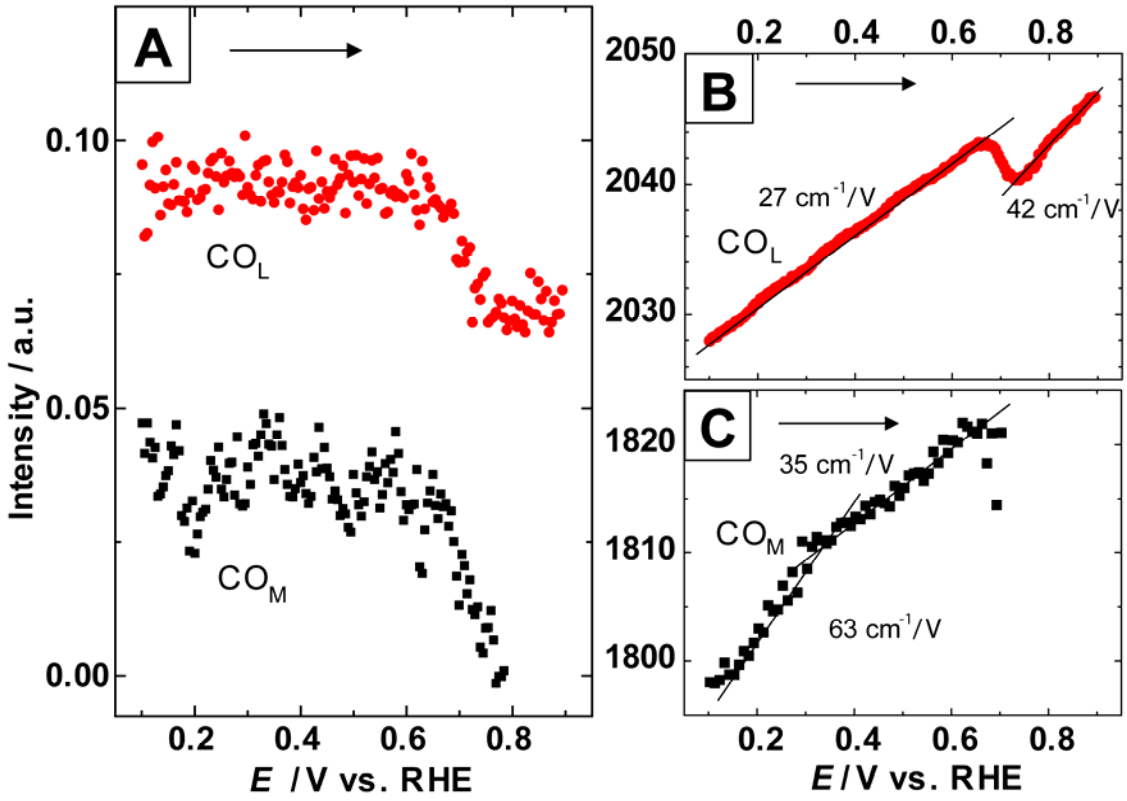
A
B
C
0.10
0.05
0.00
Intensity / a.u.
CO_L
CO_M
0.2
0.4
0.6
0.8
E /V vs. RHE
2050
2040
2030
27 cm-1/V
42 cm-1/V
1820
1810
1800
35 cm-1/V
63 cm-1/V

Figure 8

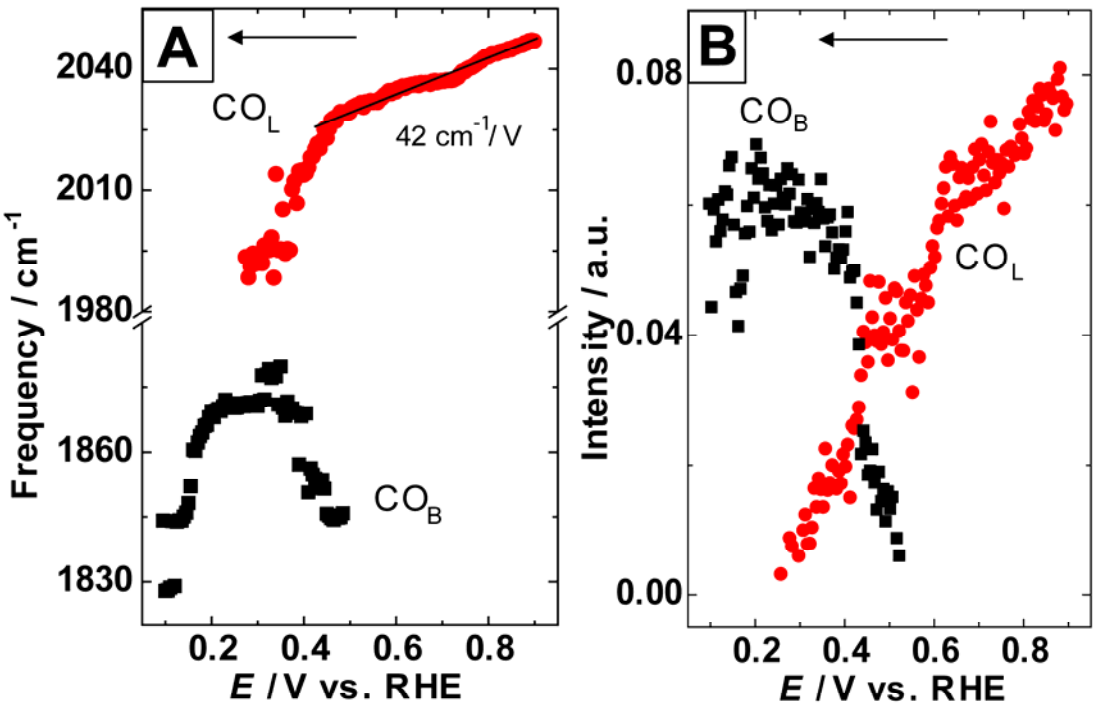
A
B
2040
2010
1980
1860
1830
Frequency / cm-1
CO_L
42 cm-1/ V
CO_B
0.2
0.4
0.6
0.8
E / V vs. RHE
0.08
0.04
0.00
Intensity / a.u.
CO_B
CO_L
0.2
0.4
0.6
0.8
E / V vs. RHE

References:

[1] N.M. Markovic, P.N. Ross, Surface science studies of model fuel cell electrocatalysts, Surf. Sci. Rep. 45 (2002) 117.
[2] H.A. Gasteiger, N.M. Markovic, P.N. Ross Jr., E.J. Cairns, Carbon monoxide electrooxidation on well-characterized platinum-ruthenium alloys, J. Phys. Chem. 98 (1994) 617.
[3] R. Parsons, T. Vandernoot, The oxidation of small organic molecules: A survey of recent fuel cell related research, J. Electroanal. Chem. 257 (1988) 9.
[4] A. Hamnett, Mechanism and electrocatalysis in the direct methanol fuel cell, Catal. Today 38 (1997) 445.
[5] A. Hamnett, The mechanism of methanol electro-oxidation, Comprehensive Chemical Kinetics 37 (1999) 635.
[6] H.S. Gandhi, G.W. Graham, R.W. McCabe, Automotive exhaust catalysis, J. Catal. 216 (2003) 433.
[7] M. Shelef, G.W. Graham, Why rhodium in automotive three-way catalysts, Catal. Rev. Sci. Eng. 36 (1994) 433.
[8] M.J.P. Hopstaken, J.W. Niemantsverdriet, Structure sensitivity in the CO oxidation on rhodium: Effect of adsorbate coverages on oxidation kinetics on Rh(100) and Rh(111), J. Chem. Phys. 113 (2000) 5457.
[9] L.W.H. Leung, S.C. Chang, M.J. Weaver, Electrochemical infrared spectroscopy of carbon monoxide on ordered rhodium (111): Comparisons with vibrational spectra on Pt(111) and in related surface-vacuum environments, J. Chem. Phys. 90 (1989) 7426.
[10] L.W.H. Leung, M.J. Weaver, Adsorption and electrooxidation of some simple organic molecules on rhodium (111) as probed by real-time FTIR spectroscopy: comparisons with platinum (111), J. Phys. Chem. 93 (1989) 7218.
[11] S.C. Chang, M.J. Weaver, The characterization of carbon monoxide electrosorbed on ordered rhodium (100) by in-situ infrared spectroscopy, J. Electroanal. Chem. 285 (1990) 263.
[12] S.C. Chang, M.J. Weaver, Coverage- and potential-dependent binding geometris of carbon monoxide at ordered low-index platinum and rhodium aqueous interfaces: comparisons with adsorption in corresponding metal-vacuum environments, Surf. Sci. 238 (1990) 142.
[13] M.J. Weaver, S.C. Chang, L.W.H. Leung, X. Jiang, M. Rubel, M. Szklarczyk, D. Zurawski, A. Wieckowski, Evaluation of absolute saturation coverage of carbon monoxide on ordered low-index platinum and rhodium electrodes, J. Electroanal. Chem. 327 (1992) 247.
[14] S.C. Chang, Y. Ho, M.J. Weaver, Coverage-dependent errors in the coulometric assay of adsorbed reactants: carbon monoxide on rhodium (100), J. Electrochem. Soc. 139 (1992) 147.
[15] S.L. Yau, X. Gao, S.C. Chang, B.C. Schardt, M.J. Weaver, Atomic-resolution scanning tunneling microscopy and infrared spectroscopy as combined in situ probes of electrochemical adlayer structure: carbon monoxide on rhodium (111), J. Am. Chem. Soc. 113 (1991) 6049.

[16] R. Gómez, J.M. Orts, J.M. Feliu, J. Clavilier, L.H. Klein, The role of surface crystalline heterogeneities in the electrooxidation of carbon monoxide adsorbed on Rh(111) electrodes in sulphuric acid solutions, J. Electroanal. Chem. 432 (1997) 1.
[17] T.H.M. Housmans, J.M. Feliu, M.T.M. Koper, CO oxidation on stepped Rh[n(111)×(111)] single crystal electrodes: a voltammetric study, J. Electroanal. Chem. 572 (2004) 79.
[18] T.H.M. Housmans, M.T.M. Koper, CO oxidation on stepped Rh[n(111)×(111)] single crystal electrodes: a chronoamperometric study, J. Electroanal. Chem. 575 (2005) 39.
[19] T.H.M. Housmans, M.T.M. Koper, CO oxidation on stepped Rh[n(111)×(111)] single crystal electrodes: Anion effects on CO surface mobility, Electrochem. Commun. 7 (2005) 581.
[20] T.H.M. Housmans, C.G.M. Hermse, M.T.M. Koper, CO oxidation on stepped single crystal electrodes: A dynamic Monte Carlo study, J. Electroanal. Chem. 607 (2007) 69.
[21] S.C.S. Lai, N.P. Lebedeva, T.H.M. Housmans, M.T.M. Koper, Mechanisms of carbon monoxide and methanol oxidation at single crystal electrodes, Top. Catal. 46 (2007) 320.
[22] Q. Xu, U. Linke, R. Bujakc, Th. Wandlowski, Preparation and electrochemical characterization of low-index rhodium single crystal electrodes in sulfuric acid, Electrochim. Acta 54 (2009) 5509.
[23] G.A. Somorjai, Introduction to Surface Chemistry and Catalysis, Wiley-Interscience, New York, 1994.
[24] R.T.S. Oliveira, M.C. Santos, L.O.S. Bulhoes, E.C. Pereira, Rh electrodeposition on Pt in acidic medium: a study using cyclic voltammetry and an electrochemical quartz crystal microbalance, J. Electroanal. Chem. 569 (2004) 233.
[25] M. Arbib, B. Zhang, V. Lazarov, D. Stoychev, A. Milchev, C. Buess-Herman, Electrochemical nucleation and growth of rhodium on gold substrates, J. Electroanal. Chem. 510 (2001) 67.
[26] G.L. Kellogg, Initial stages of oxide formation on rhodium field emitters, Phys. Rev. Lett. 54 (1985) 82.
[27] K. Tanaka, A. Sasahara, Structure and reactivity of rhodium and rhodium-based alloys, in A. Wieckowski (ed.) Interfacial Electrochemistry, Dekker, M., New York, (1999), p493-512.
[28] M. Vukovic, Electrochemical investigation of an electrodeposited rhodium electrode in acid solutions, J. Electroanal. Chem. 242 (1988) 97.
[29] J. Inukai, M. Ito, Electrodeposition processes of palladium and rhodium monolayers on Pt(111) and Pt(100) electrodes studied by IR reflection absorption spectroscopy, J. Electroanal.Chem. 358 (1993) 307.
[30] R. Gómez, A. Rodes, J.M. Perez, J.M. Feliu, A. Aldaz, Electrochemical and in situ FTIRS studies of the CO adsorption at palladium and rhodium multilayers deposited on platinum single crystal surfaces II. Pt(100) substrate, Surf. Sci. 344 (1995) 85.
[31] R. Gómez, A. Rodes, J.M. Perez, J.M. Feliu, A. Aldaz, Electrochemical and in situ FTIR studies of the CO adsorption at palladium and rhodium multilayers deposited on platinum single crystal surfaces I. Pt(110) substrate, Surf. Sci. 327 (1995) 202.
[32] R. Gómes, J.M. Feliu, Rhodium adlayers on Pt(111) monocrystalline surfaces. Eletrochemical behavior and electrocatalysis, Electrochim. Acta 44 (1998) 1191.

[33] L.A. Kibler, M. Kleinert, D.M. Kolb, The initial stages of rhodium depostion on Au(111), J. Electroanal. Chem. 467 (1999) 249.
[34] S. Zou, M.J. Weaver, Surface-enhanced Raman scattering on uniform transition-metal films: Toward a versatile adsorbate vibrational strategy for solid-nonvacuum interfaces?, Anal. Chem. 70 (1998) 2387.
[35] M. Osawa, Dynamic processes in electrochemical reactions studied by surface-enhanced infrared absorption spectroscopy (SEIRAS), Bull. Chem. Soc. Jpn. 70 (1997) 2861.
[36] M. Osawa, Surface-enhanced infrared absorption, in S. Kawata (Eds.) Near Field Optics and Surface Plasmon Polaritons, Topics Appl. Phys. 81 (2001) 163.
[37] M. Osawa, K. Ataka, K. Yoshii, Y. Nishikawa, Surface-enhanced infrared spectroscopy: The origin of the absorption enhancement and band selection rule in the infrared spectra of molecules adsorbed on fine metal particles, Appl. Spectrosc. 47 (1993) 1497.
[38] M. Osawa, K. Yoshii, In situ and real-time surface-enhanced infrared study of electrochemical reactions, Appl. Spectro. 51 (1997) 512.
[39] M. Watanabe, Y.M. Zhu, H. Uchida, Oxidation of CO on a Pt-Fe alloy electrode studied by surface enhanced infrared reflection absorption spectroscopy, J. Phys. Chem. B 104 (2000) 1762.
[40] A. Miki, S. Ye, T. Senzaki, M. Osawa, Surface-enhanced infrared study by catalytic electrooxidation of formaldehyde, methyl formate and dimethoxymethane on platinum electrodes in acidic solution, J. Electroanal. Chem. 563 (2004) 23.
[41] Y.X. Chen, M. Heinen, Z. Jusys, R.J. Behm, Kinetics and mechanism of the electrooxidation of formic acid - spectroelectrochemical studies in a flow cell, Angew. Chem. Int. Ed. 45 (2006) 981.
[42] Th. Wandlowski, K. Ataka, S. Pronkin, D. Diesing, Surface enhanced infrared spectroscopy –Au(111-20 nm)/sulphuric acid – new aspects and challenges, Electrochim. Acta 49 (2004) 1233.
[43] U. Zhumaev, A.V. Rudnev, J.F. Li, A. Kuzume, T.H. Vu, Th. Wandlowski, Electro-oxidation of Au(111) in contact with aqueous electrolytes: New insight from in situ vibration spectroscopy, Electrochim. Acta 112 (2013) 853.
[44] J. Clavilier, D. Armand, S.G. Sun, M. Petit, Electrochemical adsorption behaviour of platinum stepped surfaces in sulphuric acid solutions, J. Electroanal. Chem. 205 (1986) 267.
[45] M. Arenz, V. Stamenkovic, P.N. Ross, N.M. Markovic, Preferential oxidation of carbon monoxide adsorbed on Pd submonolayer films deposited on Pt(100), Electrochem. Commun. 5 (2003) 809.
[46] M. Arenz, V. Stamenkovic, T.J. Schmidt, K. Wandelt, P.N. Ross, N.M. Markovic, CO adsorption and kinetics on well-characterized Pd films on Pt(111) in alkaline solutions, Surf. Sci. 506 (2002) 287.
[47] K. Ataka, M. Osawa, In situ infrared study of water-sulfate coadsorption on gold (111) in sulfuric acid solutions, Langmuir 14 (1998) 951.
[48] P.A. Thiel, T.E. Madey, The interaction of water with solid surfaces: Fundamental aspects, Surf. Sci. Rep. 7 (1987) 211.
[49] M. Wolf, S. Nettersheim, J.M. White, E. Hasselbrin G. Ertl, Dynamics of the ultraviolet photochemistry of water adsorbed on Pd(111), J. Chem. Phys. 94 (1991) 4609.

[50] B. Álvarez, V. Climent, A. Rodes, J.M. Feliu, Anion adsorption on Pd-Pt(111) electrodes in sulphuric acid solution, J. Electroanal. Chem. 497 (2001) 125.
[51] Y. Yan, Q.X. Li, S.L. Huo M. Ma, W.B. Cai. M. Osawa, Ubiquitous strategy for probing ATR surface-enhanced infrared absorption at platinum group metal−electrolyte interfaces, J. Phys. Chem. B 109 (2005) 7900.
[52] M. Watanabe, T. Sato, K. Kunimatsu, H. Uchida, Temperature dependence of co-adsorption of carbon monoxide and water on highly dispersed Pt/C and PtRu/C electrodes studied by in-situ ATR-FTIRAS, Electrochim. Acta 53 (2008) 6928.
[53] K. Ataka, T. Yotsuyanagi, M. Osawa, Potential-dependent reorientation of water molecules at an electrode/electrolyte interface studied by surface-enhanced infrared absorption spectroscopy, J. Phys. Chem. 100 (1996) 10664.
[54] M. Osawa, M. Tsushima, H. Mogami, G. Samjeske, A Yamakata, Structure of water at the electrified platinum – water interface: A study by surface-enhanced infrared absorption spectroscopy, J. Phys. Chem. C 112 (2008) 4248.
[55] K. Kunimatsu, R.O. Lezna, M. Enyo, Adsorption and oxidation of carbon monoxide on a rhodium electrode studied by in-situ infrared spectroscopy, J. Electroanal. Chem. 258 (1989) 115.
[56] Y.G. Yan, Y.Y. Yang, B. Peng, S. Malkhandi, A. Bund, U. Stimming, W.B. Cai, Study of CO Oxidation on Polycrystalline Pt Electrodes in Acidic Solution by ATR-SEIRAS, J. Phys. Chem. C 115 (2011) 16378.
[57] N.P. Lebedeva, M.T.M. Koper, J.M. Feliu, R.A. Van Santen, Role of crystalline defects in electrocatalysis: Mechanism and kinetics of CO adlayer oxidation on stepped Platinum electrodes, J. Phys. Chem. B 106 (2002) 12938.
[58] K. Kunimatsu, T. Sato, H. Uchida, M. Watanabe, Role of terrace/step edge sites in CO adsorption/oxidation on a polycrystalline Pt electrode studied by in situ ATR-FTIR method, Electrochim. Acta 53 (2008) 6104.
[59] H. Miyake, T. Okada, G. Samjeské, M. Osawa, Formic acid electrooxidation on Pd in acidic solutions studied by surface-enhanced infrared absorption spectroscopy, Phys. Chem. Chem. Phys. 10 (2008) 3662.
[60] Y.Y. Yang, J. Ren, H.X. Zhang, Z.Y. Zhou, S.G. Sun, W.B. Cai, Infrared Spectroelectrochemical Study of Dissociation and Oxidation of Methanol at a Palladium Electrode in Alkaline Solution, Langmuir, 29 (2013) 1709.
[61] K.A. Friedrich, K.P. Geyzers, U. Linke, U. Stimming, J. Stumper, CO adsorption and oxidation on a Pt(111) electrode modified by ruthenium deposition: an IR spectroscopic study, J. Electroanal. Chem. 402 (1996) 123.
[62] T. Yajima, H. Uchida, M. Watanabe, In-Situ ATR-FTIR spectroscopic study of electro-oxidations of methanol and adsorbed CO at Pt−Ru alloy, J. Phys. Chem. B 108 (2004) 2654.
[63] Y. Yan, Ph. D. dissertation in Fudan University (2007).
[64] T. Iwasita, F.C. Nart, in H. Gerischer, C.W. Tobias (Eds.), Advances in Electrochem. Sci. and Engineering, vol. 4, VCH, Weinheim, (1995).
[65] R. Gómez, J.M. Feliu, A. Aldaz, M.J. Weaver, Validity of double-layer charge-corrected voltammetry for assaying carbon monoxide coverages on ordered transition metals: comparisons with adlayer structures in electrochemical and ultrahigh vacuum environments, Surf. Sci. 410 (1998) 48.
[66] Q. Xu, Ph.D. thesis, Chapter 4, University of Bern, (2010).

[67] A.B. Anderson, M.K. Awad, Factors determining carbon monoxide adsorption sites on palladium and platinum (100) and (111) surfaces: theoretical study, J. Am. Chem. Soc. 107 (1985) 7854.
[68] W. Mueller P.S. Bagus, Analyses for the C-O stretch frequency shifts of CO chemisorbed on Cu(100) in the absence and presence of an electric field, Electron Spectrosc. Relat. Phenom. 38 (1986) 103.
[69] D.K. Lambert, Stark effect of adsorbate vibrations, Solid State Commun. 51 (1984) 297.
[70] S. Gilman The Mechanism of electrochemical oxidation of carbon monoxide and methanol on Platinum. II. The "reactant-pair" mechanism for electrochemical oxidation of carbon monoxide and methanol, J. Phys. Chem. 68 (1964) 70.
[71] N.P. Lebedeva, M.T.M. Koper, J.M. Feliu, R.A. van Santen, The effect of the cooling atmosphere in the preparation of flame-annealed Pt(111) electrodes on CO adlayer oxidation, Electrochem. Commun. 2 (2000) 487.